Pergamon

Int. J. Heat Mass Transfer. Vol. 41, No. 16, pp. 2455–2467, 1998

Printed in Great Britain
0017–9310/98 $19.00+0.00

PII: S0017–9310(97)00335–9

Temperature distribution in swirling jets

V. SHTERN,† A. BORISSOV and F. HUSSAIN

Department of Mechanical Engineering, University of Houston, Houston TX 77204-4792, U.S.A.

(*Received* 20 *February* 1997 *and in final form* 23 *October* 1997)

Abstract—Analytical solutions of the energy equation are obtained showing strong effects of flow swirl: (a) significant increase in heat exchange, (b) heat isolation of a wall, (c) formation of temperature fronts and (d) flame stabilization in vortex burners. Two problems are studied in detail: (i) a point source of heat at the origin of a swirling jet submerged in an infinite fluid and (ii) heat transfer from an isothermal wall near a swirling jet. The paper explains the physical mechanism of effects (a–d) and shows the means to control them. © 1998 Elsevier Science Ltd. All rights reserved.

INTRODUCTION

Swirl significantly influences heat and mass transfer in many natural and technological flows. Swirl is used in vortex burners and chemical reactors to stabilize the flame front and to increase the surface area across which heat and mass exchange occurs [1]. In vortex devices, centrifugal acceleration can be as high as 10^4 times the gravity and provides useful stratification of temperature and density [2]. Hot low-density fluid collects near the axis of rotation, i.e., away from sidewalls, while the near-wall region consists of cold high-density fluid. Internal recirculatory domains ('bubbles'), typical of swirling flows, are favorable for stable combustion providing thermal feedback and fuel preheating [3]. Swirling fuel jets are also used to enhance mixing in scramjet engines [4]. In natural flows, such as tornadoes or firestorms, swirl induces a temperature front, i.e., a thin layer separating cold and hot air. A particularly striking result of swirl is the Ranque effect [5, 6].

Despite these and many other applications, little is known about the fundamentals of heat transfer in swirling flows. Although effects of swirl have been observed, synthesizing experimental data has proven difficult. One reason is the large number of control parameters, and another is the swirling flow sensitivity to external disturbances. For these reasons, an empirical search of optimal parameters for heat transfer is not efficient. Numerical simulations suffer from similar limitations and the additional technical difficulties related to complex flows.

Thus, analytical solutions are useful for (a) a clear understanding of the mechanism of the influence of swirl on heat transfer, (b) a detailed investigation over a wide range of control parameters and (c) optimization for a particular problem. Also, they would indicate parameters at which further experimental and numerical studies are to be carried out. Unfortunately, obtaining analytical solutions for the Navier–Stokes and heat equations is a difficult task. Rumer's solution [7] for a point heat source at the origin of the Landau jet is available, but no result has been found for convective heat transfer in swirling flows.

Recently, a family of analytical solutions describing swirling flows in conical domains, has been obtained as functions of the cone angle, circulation and flow force [8]. Here we apply and expand these solutions for heat transfer in swirling jets induced by a half-line vortex in free space and normal to a wall. The jets model tornadoes, outflows of vortex chambers, aircraft trailing vortices and near-axis flows in vortex burners. The jets have features typical of swirling flows including: (i) appearance of recirculatory zones, (ii) significant decrease in pressure near the rotation axis, and (iii) multi-stability and jump transitions between regimes [8]. Conical similarity also permits analysis of turbulent jets by interpreting viscosity as eddy (turbulent) viscosity; this has been justified for swirl-free round jets by Schlichting [9] and for swirling jets by Squire [10] and others [11–13]. One can thus interpret these solutions to be those for the mean fields of velocity and temperature in practical turbulent flows.

The paper deals with two heat transfer problems: (i) point source of heat at the origin of a swirling jet in a full space and (ii) heat transfer through a swirling jet from a wall to ambient fluid having uniform but different temperatures. These two problems allow us to elucidate the role of swirl in heat transport in jets, which is the main goal for this paper.

GOVERNING EQUATIONS

We address the Navier–Stokes equations for a steady motion of an incompressible fluid,

$$(\mathbf{v}\cdot\nabla)\mathbf{v} = \nu\Delta\mathbf{v} - \nabla p/\rho, \quad \nabla\cdot\mathbf{v} = 0 \qquad (1)$$

† Author to whom correspondence should be addressed. Tel.: 001 713 743 4554. Fax: 001 713 743 4503. E-mail: mece21w@jetson.uh.edu.

NOMENCLATURE

A	dimensionless parameter for force F
c_v	specific heat
C, C_3, C_3	integration constants
C_p	pressure coefficient
J_0	flow force
k	thermal conductivity
M	Long's parameter
Nu	Nusselt number
p, q	dimensional and dimensionless pressure
Pr	Prandtl number
Q	total heat flux from the point source
r	spherical radius
Ro_m	Rossby number—the ratio of maximal radial/swirl velocities
Re	Reynolds number
$Sr = Ro_m^{-1}$	swirl number
t, T	dimensionless and dimensional temperature
$\mathbf{v}$, v, V	velocity vector and its components
u, w	scaled radial and swirl velocities
x, y	dimensionless coordinates
z	axial coordinate.

Greek symbols

Γ	circulation
η, ξ	scaled polar angle
θ, ϕ	polar and azimuthal angles
ϑ	dimensionless temperature
ν	kinematic viscosity
ρ	density
ψ, Ψ	dimensionless and dimensional stream function
∇, Δ	gradient and Laplacian.

Subscripts

a	axial
m	maximum value
s	swirl
1, 2, b	quantities related to regions 1, 2 and boundary layer.

and conical similarity flows which have the representation,

$$v_r = -v\psi'(x)/r; \quad v_\theta = -v\psi(x)/(r\sin\theta),$$

$$v_\phi = v\Gamma(x)/(r\sin\theta) \quad p = p_\infty + \rho v^2 q(x)/r^2,$$

$$\Psi = vr\psi(x), \quad x = \cos\theta. \tag{2}$$

Here (r, θ, ϕ) are the spherical coordinates (see Fig. 1); (v_r, v_θ, v_ϕ), p and Ψ are velocity components, pressure and the Stokes stream function; ψ, Γ and q are dimensionless functions; and the prime denotes differentiation with respect to x. Using (2) reduced (1) to the system of ordinary differential equations (ODE),

$$(1-x^2)\psi' - 2x\psi - \tfrac{1}{2}\psi^2 = F \tag{3a}$$

$$(1-x^2)F''' = 2\Gamma\Gamma' \tag{3b}$$

$$(1-x^2)\Gamma'' = \psi\Gamma' \tag{3c}$$

where the auxiliary function F defined by (3b) replaces q (see ref. [8] for more details).

Next, we study heat transport in conical flows by considering the energy equation, $\rho c_v(\mathbf{v}\cdot\nabla)T = k\Delta T + S$, in the spherical coordinates [14]:

$$\rho c_v\{v_r\partial T/\partial r + r^{-1}v_\theta\partial T/\partial\theta + (r\sin\theta)^{-1}v_\phi\partial T/\partial\phi\}$$
$$= k\{r^{-2}\,\partial/\partial r(r^2\,\partial T/\partial r) + (r^2\sin\theta)^{-1}\partial/\partial\theta$$
$$\times(\sin\theta\,\partial T/\partial\theta) + (r\sin\theta)^{-2}\partial^2 T/\partial\phi^2\} + S \tag{4a}$$

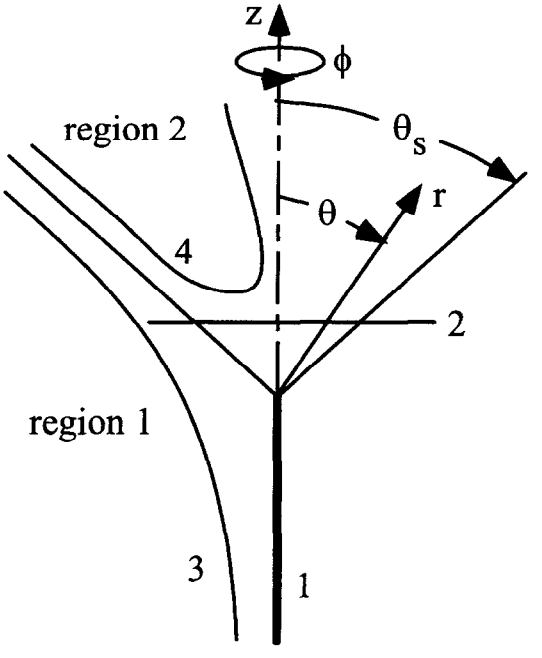

Fig. 1. Schematic of the problem. Half-line vortex 1 is characterized by circulation Re_s and flow force J_0 given on plane 2 normal to the line vortex. There are two flow cells separated by conical surface $\theta = \theta_s$. Curves 3 and 4 show typical streamlines of the meridional motion. (r, θ, ϕ) are the spherical coordinates.

where S denotes a heat source. Using (2) reduces (4a) to

$$[(1-x^2)T']'+(1-x^2)^{-1}T_{\phi\phi}+T_{\xi\xi}+T_{\xi}$$
$$+Pr\{\psi' T_{\xi}-\psi T'-\Gamma(1-x^2)^{-1}T_{\phi}\}+s=0 \quad (4b)$$

where $s=r^2S/k$, $\xi=\ln r$, $Pr=\rho c_v v/k$, and the indices denote differentiation with respect to ξ and ϕ. We consider Pr and s independent of T, and, therefore, (4b) is a linear equation. Since the coefficients of (4b) are functions of x only, the Laplace–Fourier transformation with respect to ξ and ϕ reduces (4b) to ODE. A general three-dimensional (3-D) temperature field can be represented as a superposition of the normal modes,

$$T_{m_\alpha}=\vartheta_{m_\alpha}(x)\exp(\alpha\xi+im\phi). \quad (5)$$

Here $m=0,\pm1,\pm2,\ldots$, α is a complex number, and ϑ_{m_α} is governed by the equation

$$[(1-x^2)\vartheta'_{m_\alpha}]'+[\alpha^2+\alpha-m^2(1-x^2)^{-1}]\vartheta_{m_\alpha}$$
$$+Pr\{[\alpha\psi'-im\Gamma(1-x^2)^{-1}]\vartheta_{m_\alpha}-\psi\vartheta'_{m_\alpha}\}+s_{m_\alpha}=0 \quad (6)$$

where s_{m_α} is the normal-mode projection of s. Thus, owing to conical similarity of the flow, a 3-D heat problem is reduced to decoupled equations (6) for ϑ_{m_α} which significantly simplifies the analysis. In fact, analytical solutions can be obtained, as shown in this paper. Thus, this approach provides a powerful method to solve a variety of thermal problems. Here we consider a few examples of both fundamental and practical interest.

POINT SOURCE OF HEAT IN A SWIRLING JET

The physical nature of a point heat source at the jet origin is specific to the flow. Practical examples include a hot jet issuing from a chimney into cold ambient air, firestorms, and thermal upflow above the ground heated by solar radiation. One more application is the temperature distribution in a tornado. A bulge is often observed at the mid-height of a tornado funnel [12]. Buoyancy drives up warm air from the ground to the bulge along the funnel. Above the bulge, the vortex-breakdown flow transports heat to ambient cold air. The tornado funnel below the bulge can be modeled by a half-line vortex [8] with the heat source positioned at the tip of the vortex.

Swirling jet

Figure 1 shows a schematic of the problem. The half-line vortex 1 is located at $\theta=\pi$, i.e. $x=-1$. The dimensionless control parameters are the flow force, J_0, acting on plane 2, $z=r\cos\theta=\text{const}>0$, and the vortex circulation (Γ at $x=-1$) which is denoted here as the swirl Reynolds number Re_s. Curves 3 and 4 show the meridional section of typical stream surfaces. A useful characteristic is $Re_a=-\psi'(1)=rv_a/v$, v_a is the velocity on the free part of the symmetry axis, $x=1$. This problem is solved numerically for finite J_0 and Re_s using the algorithm reported in Section 2 of ref. [8]. In this paper, we concentrate only on the results needed for the thermal problems considered.

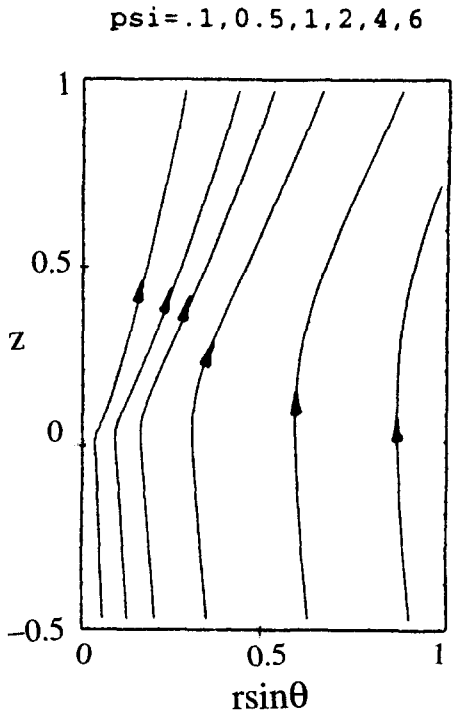

Fig. 2. Meridional streamlines of the one-cell flow at circulation $Re_s=20$ and axial velocity $Re_s=0$.

The flow can be viewed as a superposition of the meridional motion and swirl. The swirl distribution is simple: circulation is uniform on conical surfaces $x=\text{const}$ and its value monotonically decreases from $\Gamma=Re_s$ to $\Gamma=0$ as x goes from -1 to 1. A pattern of the meridional motion is more complicated: it can be one-cellular (Fig. 2) or two-cellular (Fig. 3) depending on Re_s and J_0. The surface, $\theta=\theta_s$ (where $\psi=0$), separates the flow cells (see Figs. 1 and 3).

As $Re_s\to\infty$, a strong jet develops which is consolidated near either the axis, $x=1$ (Fig. 2), or the separating surface, $x=x_s=\cos\theta_s<1$ (Fig. 3). This jet is a viscous layer while the flow outside the jet is inviscid. The corresponding solutions of the Euler and boundary layer equations for the two-cell flow (Fig. 3) are [8]:

$$\psi=\psi_1=\tfrac{1}{2}Re_s\{(1+x)[3x_s+1-(3+x_s)x]/(1+x_s)\}^{1/2} \quad (7a)$$

$$q=q_1=-\tfrac{1}{4}Re_s^2[3x_s+1-(1-x_s)x]/[(1+x_s)(1-x^2)] \quad (7b)$$

for the inviscid vortical flow in $-1<x<x_s$ (region 1 in Fig. 1) and

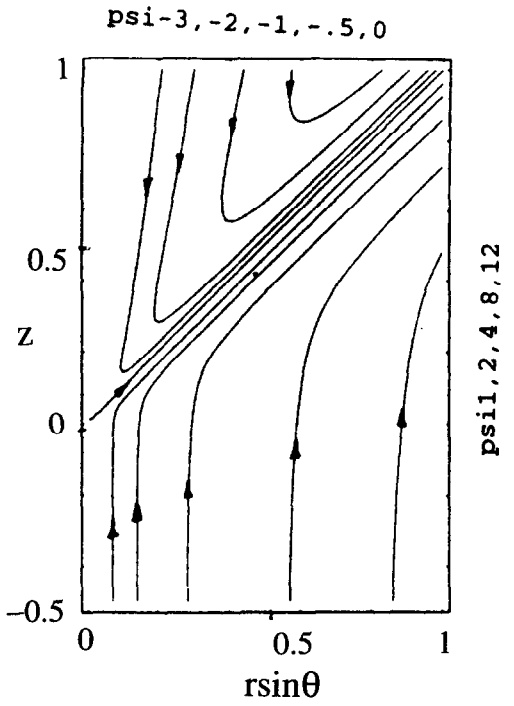

Fig. 3. Meridional streamlines of the two-cell flow at $Re_s = 20$ and $\theta_s = 45°$.

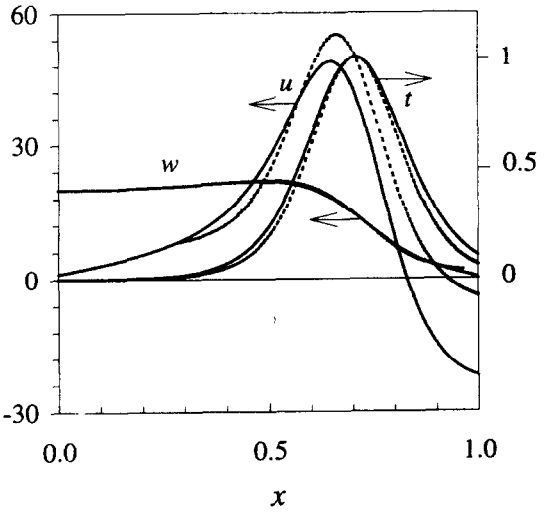

Fig. 4. The numerical (solid lines) and analytical (dotted lines) profiles of the radial u, swirl w velocities and temperature t on a sphere $r = \text{const}$ at $Re_s = 20$, $\theta_s = 45°$ and $Pr = 1$.

$$\psi = \psi_2 = -\tfrac{1}{2} Re_s (1-x)[(1+x_s)/(1-x_s)]^{1/2} \quad (8a)$$

$$q = q_2 = -\tfrac{1}{4} Re_s^2 (1+x_s)/[(1+x)(1-x_s)] \quad (8b)$$

for the irrotational flow in $x_s < x \leqslant 1$ (region 2 in Fig. 1). The boundary layer solution in the vicinity of $x = x_s$ is

$$\psi = \psi_b = -\tfrac{1}{2} Re_s (1-x_s^2)^{1/2} \tanh \xi,$$

$$\xi = \tfrac{1}{4} Re_s (x-x_s)/(1-x_s^2)^{1/2} \quad (9a)$$

$$q = q_b = -\tfrac{1}{4} Re_s^2 [x_s + (1-x_s)\tanh^2 \xi]/(1-x_s) \quad (9b)$$

and

$$\Gamma = \tfrac{1}{2} Re_s (1 - \tanh \xi). \quad (9c)$$

Solution (9c) is also a uniform approximation for swirl in the entire region, $-1 < x < 1$.

Although (7)–(9) are deduced for $Re_s \gg 1$, these solutions well approximate the flow even for moderate values of Re_s. Figure 4 shows the numerical (solid lines) and asymptotic (dotted lines) results for the radial $u = rv_t/\nu$ and swirl $w = rv_\phi/\nu$ velocities at $Re_s = 20$ with $x_s = 0.707$ ($\theta_s = 45°$). This x_s value is of especial interest since it corresponds to the maximal thrust of the swirling jet [8]. While the numerical and analytical results for w coincide within the accuracy of the drawing in Fig. 4, the results for u are different. A reason is that $u = -\psi'$ and, as usual, a difference is derivatives is larger than that in functions.

Heat problem formulation

Since the heat flux from the source is invariant for any surface surrounding the origin, temperature has the representation,

$$T = T_\infty + Q\vartheta(x)/(4\pi kr) \quad (10)$$

where T_∞ is the ambient temperature, Q is the total heat flux from the source, and ϑ is a dimensionless function satisfying the integral condition,

$$\int_{-1}^{1} \vartheta(1 - Pr\,\psi')\,dx = 2. \quad (11)$$

Substituting $\alpha = -1$, $m = 0$, $s_{m_x} = 0$ and omitting the indices in (6) yield the equation:

$$[(1-x^2)\vartheta']' = Pr(\psi\vartheta)'$$

which can be integrated to

$$(1-x^2)\vartheta' = Pr\,\psi\vartheta \quad (12)$$

where the integration constant is taken as zero for temperature to be bounded on the axis, $x = 1$. To numerically calculate a temperature distribution, at first, we integrate (12) from $x = 1$ with $\vartheta(1) = 1$ to $x = -1$. Solving the '0/0' indeterminacy in (12) at $x = 1$ yields

$$\vartheta'(1) = -Pr\,\psi'(1)/2. \quad (13)$$

After the integration, we rescale ϑ to satisfy (11). At $Pr = 0$, the solution is $\vartheta \equiv 1$ corresponding to heat conduction only. At $Pr \neq 0$ and moderate Re_s, we find solutions of (12) numerically.

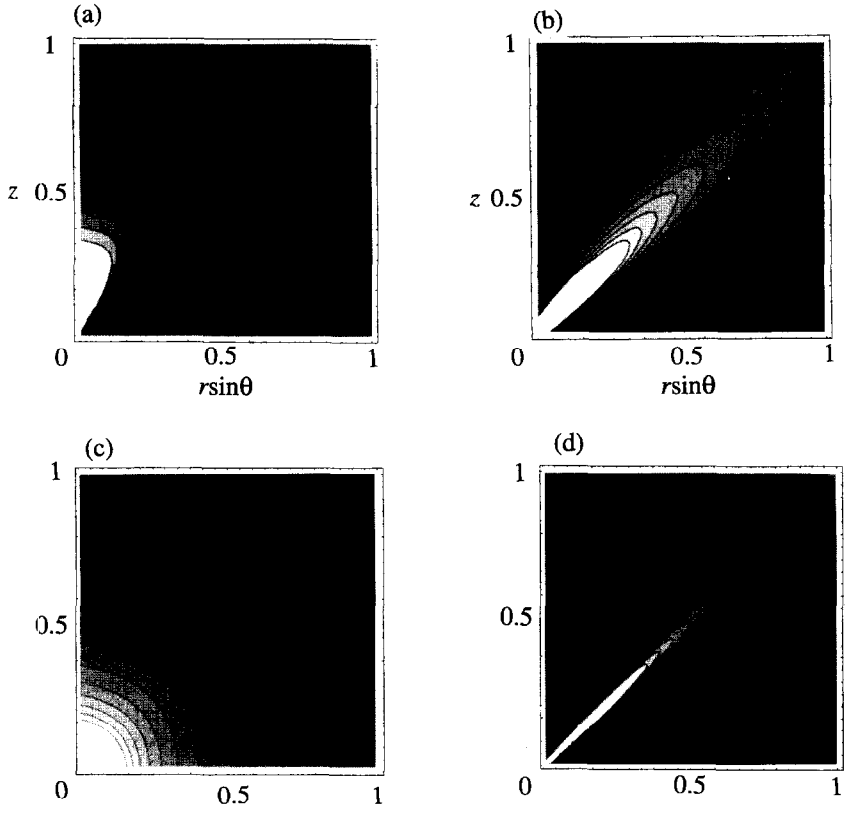

Fig. 5. Isotherms for (a) one-cell flow (Fig. 2) at $Pr = 1$, and for the two cell flow (Fig. 3) at $Pr = 1$ (b), 0.01 (c), and 7 (d).

Numerical results

Figure 5 shows isotherms for a few specific parameter values. Figure 5(a) and (b) are obtained at $Pr = 1$ for (a) one-cell flow shown in Fig. 2 and (b) two-cell flow shown in Fig. 3; the plume is consolidated near the axis in Fig. 5(a) and has the annular conical shape in Fig. 5(b). The surface area of the annular plume is significantly larger than that for the consolidated plume. This fact is very important for applications since the large plume surface provides better heat and mass transfer.

Figure 5(c) and (d) correspond to the same flow as Fig. 5(b) but for (c) $Pr = 0.01$ and (d) $Pr = 7$ (these Pr values are typical for liquid metals and water, respectively). The plume thickness depends on Pr as usual: isotherms are nearly spherical surfaces in Fig. 5(c) since the contribution of convection to heat transfer is negligible in comparison with that from conduction [at $Pr = 0, \vartheta \equiv 1$ as follows from (11) and (12)]. In contrast, the plume in Fig. 5(d) is significantly thinner than the annular jet, and the contribution from convection dominates that from conduction.

While these numerical results illustrate the influence of swirl at particular parameter values, the following analytical solutions provide some general relations for heat transfer.

Analytical solution for temperature in the two-cell flow

Substituting ψ and ξ from (9a) in (12) and allowing $Re_s \to \infty$, we get

$$\vartheta' = -2\,Pr\,\vartheta \tanh \xi \tag{14}$$

where the prime denotes the differentiation with respect to ξ. Integrating (14) yields

$$\vartheta = \vartheta_m (\cosh \xi)^{-2Pr} \tag{15}$$

where ϑ_m is an integration constant (and the maximal value of ϑ) to be found. Since $\vartheta_m = 1$ at $Pr = 0$ and ϑ_m decreases as heat transfer increases at fixed Q, the value of ϑ_m^{-1} characterizes a total/conduction heat transfer ratio. To find ϑ_m for $Pr \neq 0$ and large Re_s, we use the asymptotic form of (11) as $Re_s \to \infty$, which is

$$Pr\,Re_s \int_{-\infty}^{\infty} \vartheta (\cosh \xi)^{-2}\,d\xi = 4(1-x_s^2)^{-1/2}$$

and (15), resulting in

$$\vartheta_m^{-1} = \tfrac{1}{4} Pr\,Re_s (1-x_s^2)^{1/2} A(Pr),$$

$$A(Pr) = \int_{-\infty}^{\infty} (\cosh \xi)^{-2-2Pr}\,d\xi. \tag{16}$$

Function $A(Pr)$ (which can be expressed in terms of the Euler gamma function) monotonically decreases as Pr increases. In particular, $A(0) = 2$, $A(1) = 4/3$, and $A(Pr) \to (\pi/Pr)^{1/2}$ as $Pr \to \infty$.

When one models turbulence with the help of eddy viscosity and heat diffusivity, the case $Pr = 1$ is interesting since it is a typical value for the turbulent Prandtl number. For this case,

$$\vartheta_m^{-1} = Re_s(1-x_s^2)^{1/2}/3 \tag{17}$$

as follows from (16). Thus, ϑ_m^{-1} (i.e. heat transfer efficiency) increases proportionally to the swirl Reynolds number Re_s at fixed x_s.

According to (15), temperature exponentially decays, $\vartheta = \vartheta_m 2^{2Pr}\exp(-2\,Pr|\xi|)$, as $|\xi| \to \infty$. A similar decay in the boundary layer solution for the radial velocity means only that u, being $O(Re_s^2)$ inside the annular jet, becomes of $O(Re_s)$ outside the jet. To find the temperature outside the jet, one needs to solve the heat equation for the inviscid flow regions. Consider, for example, region 2 in Fig. 1 where the flow is irrotational (this problem is simpler than that for region 1). Substituting (8a) and (12) and integrating yield

$$\vartheta = C(1+x)^b, \quad b = -\tfrac{1}{2}Pr\,Re_s[(1-x_s)/(1+x_s)]^{1/2}$$

where the integration constant C is found by matching this solution with (15). This gives $C = \vartheta_m 2^{2Pr}/(1+x_s)^b$ which means that in the irrotational flow, the temperature decays exponentially with respect to Re_s as $Re_s \to \infty$. A similar results is obtained (from lengthy calculations omitted) for the vortical inviscid region. Thus, (15) is an excellent uniform approximation for the temperature in the entire region, $-1 \leqslant x \leqslant 1$.

Figure 4 shows the numerical (solid curve) and analytical (dotted curve) results for the normalized temperature, $t = \vartheta/\vartheta_m$, at $Pr = 1$, $Re_s = 20$ and $x_s = 0.707$. One can see that the asymptotic solution is close to the numerical one despite Re_s not being too large. Also Fig. 4 shows that the profiles of the radial velocity u and temperature t are similar but relatively shifted. The radial velocity profile in the annular jet is $u = Re_m\cosh^{-2}\xi$, $Re_m = Re_s^2/8$, as it follows from differentiation of (9a). Comparing this profile with (15) at $Pr = 1$, one can see that the Reynolds analogy is valid for distributions of the longitudinal velocity and temperature in the boundary layer limit. The difference between u and t in Fig. 4 is mainly due to a shift in the locations of the maxima. It follows from (12) that ϑ is maximum where $\psi = 0$, i.e. exactly at $x = x_s$. On the other hand, u reaches its maximum at $x_m = x_s - 4(1+x_s)(1-x_s^2)/Re_s^2$ as $Re_s \to \infty$ [8]. Note that the difference $x_s - x_m$ at $Re_s = 20$ (Fig. 4) is larger than the asymptotic estimate. Nevertheless, the Reynolds analogy is valid for the two-cell swirling flow as $Re_s \to \infty$. In contrast, the Reynolds analogy is not valid for the Long jet as we show below.

Temperature distribution in the Long jet

The near-axis jet develops as $Re_s \to \infty$ and $x_s = 1$ or $x_s \to 1$. This jet was studied by Long [15] using the boundary layer approximation. Outside the jet, the irrotational region 2 (Fig. 1) disappears and the vortical region 1 now occupies the entire interval $-1 < x < 1$, where the inviscid solution is

$$\psi = Re_s[(1-x^2)/2]^{1/2}, \quad \Gamma \equiv Re_s$$

$$\text{and} \quad q = -\tfrac{1}{2}Re_s^2/(1-x^2). \tag{18a–c}$$

According to (18), velocity and pressure are unbounded on the axis, so viscosity cannot be neglected in the vicinity of $x = 1$. The boundary-layer approach yields that all quantities are bounded and, in particular, $u \sim O(Re_s^2)$ and $q \sim O(Re_s^4)$. The inner variable is $\eta = Re_s^2(1-x)$ [8] or $y = \eta^{1/2}$ [15]. The Long number, $M = 2\pi J_0/Re_s^2$, is the single controlling parameter as $Re_s \to \infty$. Important resulting characteristics (presented in Fig. 6) are $V_{rm} = Re_m/Re_s^2$ (Re_m is the maximum value of u), $V_a = Re_a/Re_s^2$ and the pressure coefficient C_p which is the ratio of the pressure drop to the dynamic head, $C_p = 2(p_\infty - p_a)/(\rho v_{rm}^2)$, where p_a is pressure on the axis and v_{rm} is the maximal radial velocity at a fixed r. Note that despite p_a and v_m being dependent on r, C_p is an r-independent (i.e. global) flow characteristic.

As Long [15] found, there is a fold at $M = M_f = 3.74$ and two boundary layer solutions for each $M > M_f$ (Fig. 6). The one-cell flow ($V_a > 0$) corresponds to the upper solution branch and the flow is two-cellular on the lower branch (except in the vicinity of the fold point). The maximum radial velocity is located on the axis (i.e., $V_{rm} = V_a$) to the right of symbol '×' on the upper branch. As $M \to \infty$, the Long jet transforms to the Schlichting round jet [9] along the upper branch and to the annular conical jet along the lower branch in Fig. 6. Figure 7 shows the velocity profiles, $V_r = u/Re_s^2$ and $V_\phi = w/Re_s^2$, at points a–d in Fig. 6.

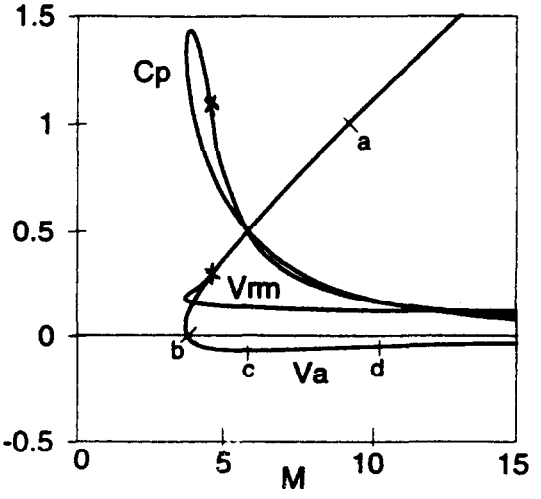

Fig. 6. Pressure coefficient C_p, axial V_a and maximal radial V_{rm} velocities as functions of the normalized flow force M in the Long boundary layer.

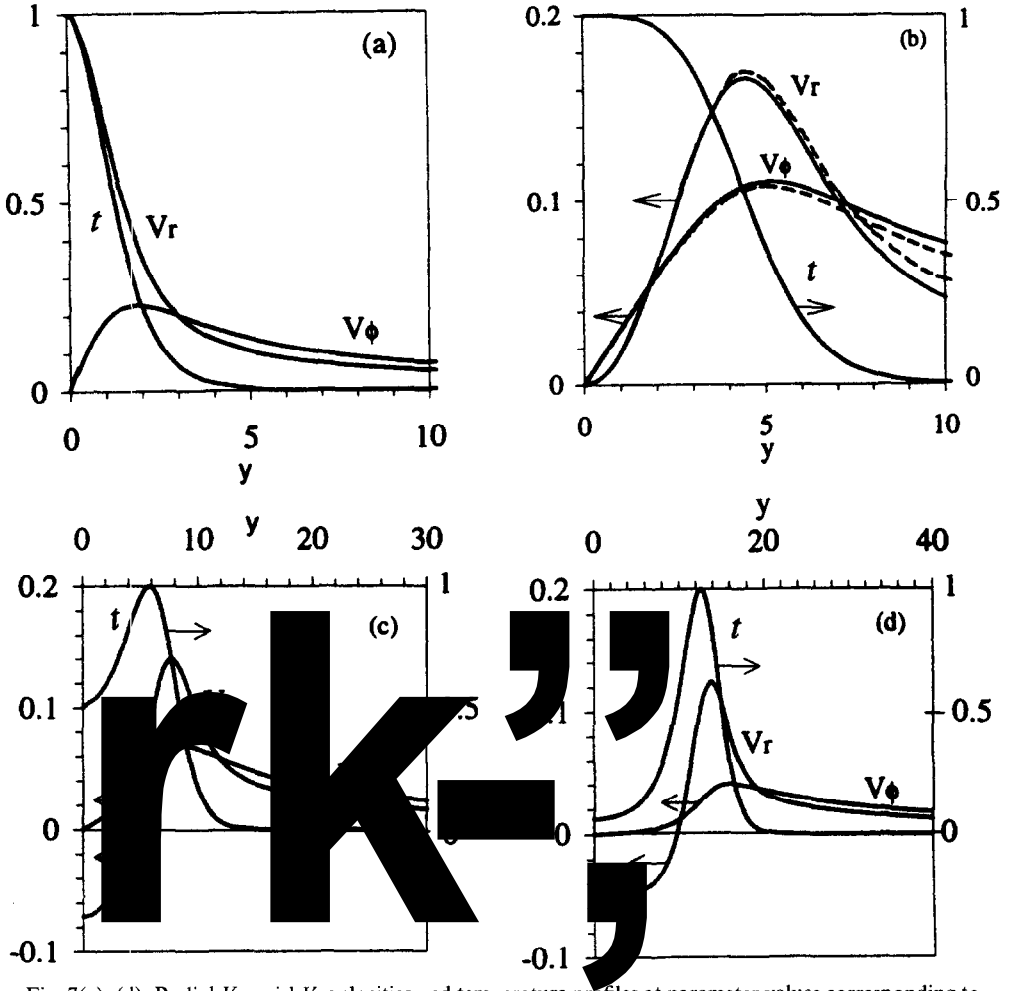

Fig. 7(a)–(d). Radial V_r, swirl V_ϕ velocities and temperature profiles at parameter values corresponding to points a–d Fig. 6 and $Pr = 1$. The broken curves in (b) show the numerical results for the entire space problem at $Re_s = 20$.

Consider the heat problem for the Long jet. Substituting $\eta = Re_s^2(1-x)$ in (12) and allowing $Re_s \to \infty$ yield the boundary layer equation for temperature:

$$\eta\vartheta' = -\tfrac{1}{2}Pr\psi\vartheta$$

where the prime denotes differentiation with respect to η and ψ is a solution of the Long problem. Integrating gives

$$\vartheta = \vartheta_a \exp\left\{-\frac{1}{2}Pr\int_0^\eta \psi\eta^{-1}\,d\eta\right\} \qquad (19)$$

where ϑ_a is the ϑ value at the axis, $\eta = 0$. Note that (19) is not an analytical solution because there is no analytical expression for ψ. Curves $t = \vartheta/\vartheta_m$ in Fig. 7 show the numerical solutions of (19) at $Pr = 1$ for the corresponding flow fields.

One can see that the profiles of t and V_r are qualitatively different. In Figs 7(c–d), V_r is negative near the axis while t is, of course, positive. In Fig. 7(b), the V_r maximum is located away from the axis while temperature maximum is on the axis. Although, the profiles of t and V_r appear similar for small y in Fig. 7(a), they are very different as $y = \to \infty$. While $V_r \to 1/(2y)$ [15], (19) yields that $\vartheta \sim \exp(-Pr\,y)$; i.e. ϑ decays significantly faster than V_r as $y \to \infty$.

The fact that the Reynolds analogy is not valid in the Long boundary layer is due to the strong influence of the centrifugal force on the meridional motion. This effect is small near the axis where the meridional motion dominates swirl as shown in Fig. 7(a), but is large far from the axis. This occurs owing to different asymptotic behavior as the distance from the axis, $r\sin\theta$, goes to infinity; the swirl velocity decays as $(r\sin\theta)^{-1}$ while the longitudinal velocity decays as $(r\sin\theta)^{-4}$ in the Schlichting jet.

Figure 8 shows dependencies of (a) ϑ_m (the maximum temperature at a fixed r) on the Long parameter M and (b) ϑ_m^{-1} (total/conduction heat transfer ratio) on the Rossby number $Ro_m = v_{rm}/v_{\phi m}$, where $v_{\phi m}$ is the maximal swirl velocity at a fixed r. The solid curves represent the numerical results and the dashed

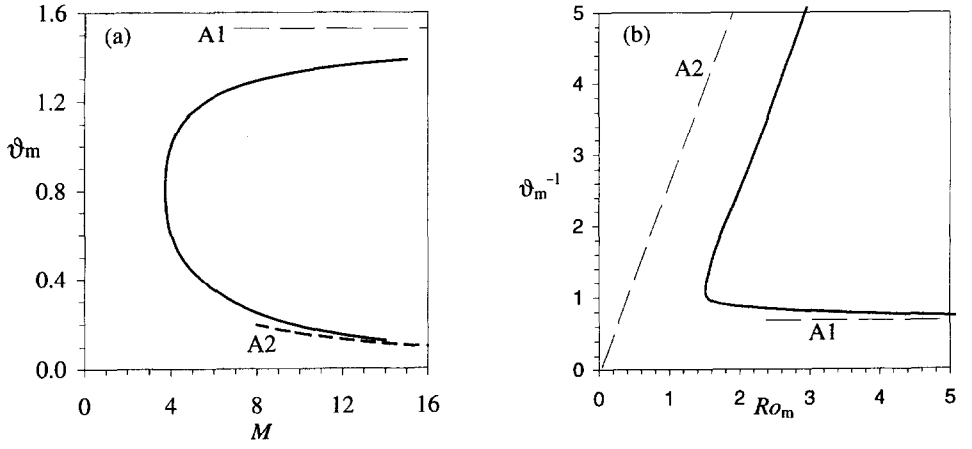

Fig. 8. (a) Maximal temperature ϑ_m at $r = \text{const}$ as a function of Long's parameter M, and (b) $1/\vartheta_m$ vs. Rossby number Ro_m at $Pr = 1$. Curves A1 and A2 are the asymptotes (23) and (20).

curves are analytical asymptotes at $Pr = 1$. For an arbitrary value of Pr, (16) yields the asymptote,

$$\vartheta_m^{-1} = 3Pr\,MA(Pr)/(2\pi) \quad \text{as } M \to \infty, \qquad (20)$$

which become $\vartheta_m = \frac{1}{2}\pi/M$ at $Pr = 1$ (line A2 in Fig. 8(a)) and can be also written as $\vartheta_m^{-1} = 8Ro_m/3$ (line A2 in Fig. 8(b)).

Lines A1 in Fig. 8(a) and (b) show the asymptote as $M \to \infty$ when the Long jet transforms into the round Schlichting jet. Using $\xi = Re_a(1-x)/4$ in (12) and allowing $Re_a \to \infty$ we have

$$\xi\vartheta' = -\tfrac{1}{2}Pr\,\psi\vartheta \qquad (21)$$

where the prime denotes differentiation with respect to ζ. Substituting the Schlichting solution, $\psi = 4\zeta/(1+\zeta)$, in (21) and integrating yield

$$\vartheta = \vartheta_m(1+\xi)^{-2Pr} \qquad (22)$$

where the maximal temperature ϑ_m is an integration constant. Note that (22) coincides with Rumer's solution [7]. Applying the normalizing condition (11) we obtain

$$\vartheta_m = 1 + 1/(2Pr) \quad \text{or } \vartheta_m^{-1} = 2Pr/(1+2Pr) \qquad (23)$$

which corresponds to lines A1 in Fig. 8(a) and (b) at $Pr = 1$. It follows from (23) that $\vartheta_m^{-1} \to 1$ as $Pr \to \infty$ and $\vartheta_m^{-1} < 1$ for finite Pr, e.g. $\vartheta_m^{-1} = 2/3$ at $Pr = 1$.

Thus, ϑ_m^{-1} for the Schlichting jet is less than that for the heat conduction ($\vartheta_m^{-1} = 1$). A reason for this surprising result is that heat spreads through a spherical surface in the heat conduction case but in the Schlichting jet, only a small cross-section is involved. Outside the jet, the entrained flow transports heat back to the source, balancing heat diffusion and thus locking heat inside the jet. The increase in heat transfer due to convection by the jet does not compensate for the decrease in heat-exchange area. It is worth noting that this effect occurs in the swirl-free flow. Swirl drastically changes the temperature distribution. As it follows from (17) $\vartheta_m^{-1} \to \infty$ as $Re_s \to \infty$, and, therefore, swirl radically enhances heat exchange. It occurs despite temperature decaying exponentially in the normal-to-flow direction in the swirling jet which is faster than the power law decay in the Schlichting jet. The swirl-induced increase in heat transfer is owing to the fact that the jet becomes annular with its cross-section area being larger ($Re_m^{1/2}$ times) than that for the Schlichting jet. Thus, our solution explicitly shows that swirl is a powerful means to intensify heat transfer. The fact that swirl induces a strong drop in the maximal temperature as the distance from the heat source increases, can be utilized to make shorter thermal wakes of practical devices (e.g., submarines). Also, swirl plays the crucial role in heat transfer from a wall as the next problem shows.

HEAT TRANSFER IN A NEAR-WALL SWIRLING JET

Features of the near-wall jet

A near-wall swirling jet is a three-dimensional boundary layer similar to those developing on swept wings of modern aircraft and in vortex combustion chambers. All velocity components are non-zero inside the boundary layer. As the distance from the wall increases, the swirl velocity tends to its non-zero ambient value (corresponding to the streamwise velocity on swept wings) and the radial velocity tends to zero (corresponding to the cross-flow velocity on swept wings). Such an analogy is the primary motivation for considering near-wall swirling flows, e.g. numerous studies of flow over rotating disks starting from ref. [16].

Though both conical and disk flows model near-wall swirling flows, there is an important distinction: the tangential velocity is directly proportional to the distance from the rotation axis in the disk flow but inversely proportional to this distance in conical flows,

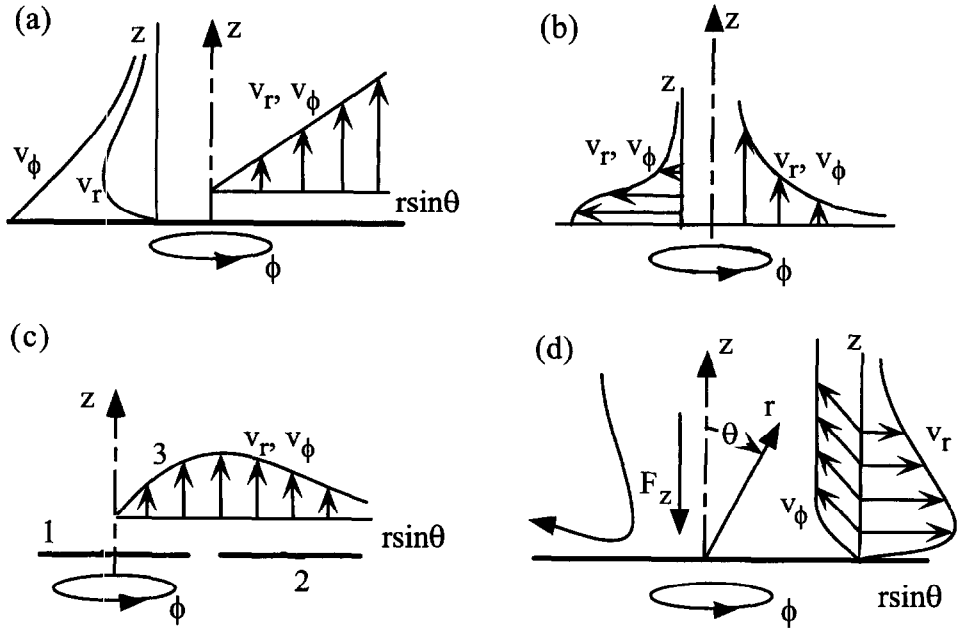

Fig. 9. Schematic of flows (a) near a rotating disk, (b) in a free radial swirling jet, (c) near disk 1 adjacent to fixed rigid wall 2. Curve 3 in Fig. 9(c) shows distribution of the swirl, v_ϕ, or radial v_r, velocity above the disk and wall at a fixed z. (d) Problem schematic for the near-wall swirling jet. A half-line vortex and axial force F_z on the axis, $\theta = 0$, induce a flow whose typical streamline and velocity profiles, $v_\phi(z)$ and $v_r(z)$ at a fixed $r\sin\theta$, are shown.

as Fig. 9(a) and (b) illustrate. Figure 9(a) shows the dependence of v_ϕ and v_r on the distance, $r\sin\theta$, from the axis (on the right side) and on z (on the left side) in the disk flow. Figure 9(b) shows similar dependencies for a conically similar swirling jet fanning along the symmetry plane, $\theta = 90°$. Figure 9(c) shows the dependence of v_ϕ and v_r (curve 3) on $r\sin\theta$ in a flow over rotating disk 1 adjacent to fixed rigid wall 2; v_ϕ and v_r grow proportionally to $r\sin\theta$ over the disk and decay as $(r\sin\theta)^{-1}$ over the wall as $r\sin\theta$ increases. For a stagnation flow induced by a swirling jet of radius r_j impinging normal to a wall, the disk and conical flows describe the near ($r\sin\theta/r_j < 1$) and far ($r\sin\theta/r_j \gg 1$) fields, respectively.

The far field can be modeled by Serrin's vortex [13]. Figure 9(d) shows the problem schematic for this conical flow. Sources of fluid motion are a half-line vortex of circulation $\nu\, Re_s$ located on the axis, $x = 1$, and force $F_z = 4\pi\nu^2 r^{-1}A$ directed along the axis. There are a typical streamline of the meridional flow and profiles of the swirl, $v_\phi(z)$, and radial, $v_r(z)$, velocities at a fixed $r\sin\theta$. Two dimensionless control parameters, Re_s and A, characterize the swirling and meridional motions. Here we consider the case where force F_z is directed downward, i.e. $A < 0$, inducing a downflow near the axis and a diverging flow near the wall (Fig. 9(d)).

As $A \to \infty$, a strong viscous jet develops near the wall while the flow outside the jet becomes asymptotically inviscid. The inviscid solution of (3) for this problem is

$$\Gamma \equiv Re_s, \quad F = 2Ax(1-x) \tag{24}$$

$$\psi = -2[-Ax(1-x)]^{1/2}. \tag{25}$$

According to (24), circulation Γ is uniform in $0 < x \leqslant 1$, and, according to (25), radial velocity $u = -\psi'$ is unbounded at $x = 0$. For this reason, a viscous boundary layer must develop to meet the no-slip condition on the wall. Consider a strong swirling jet (i.e., suppose that $Re_s \to \infty$ as $A \to -\infty$) and introduce the inner variables by scaling:

$$\gamma = \Gamma/Re_s, \quad \Phi = -F/Re_s,$$

$$W = -\psi/Re_s^{1/2}, \quad \eta = x\,Re_s^{1/2}, \tag{26}$$

where η is the dimensionless distance from the wall; W, W' and γ are the scaled normal, radial and swirl velocities, respectively. Using (26) and allowing $Re_s \to \infty$ reduce (3) to

$$W' = \Phi - W^2/2, \quad \Phi'' = 1-\gamma^2, \quad \gamma'' = -W\gamma' \tag{27}$$

where the prime denotes differentiation with respect to η. A solution of (27) must satisfy the no-slip condition on the wall, $W(0) = \Phi(0) = \gamma(0) = 0$.

To start integration from $\eta = 0$, $\Phi'(0)$ and $\gamma'(0)$ are also needed. First, we take some tentative values of $\Phi'(0)$ and $\gamma'(0) = \gamma'_w$ and integrate the initial-value problem for (27). Matching of the obtained solution with (25) requires that $\gamma \to 1$ as $\eta \to \infty$. To satisfy this condition, $\Phi'(0)$ is adjusted by the shooting procedure. In contrast, γ'_w stays a free parameter. The physical

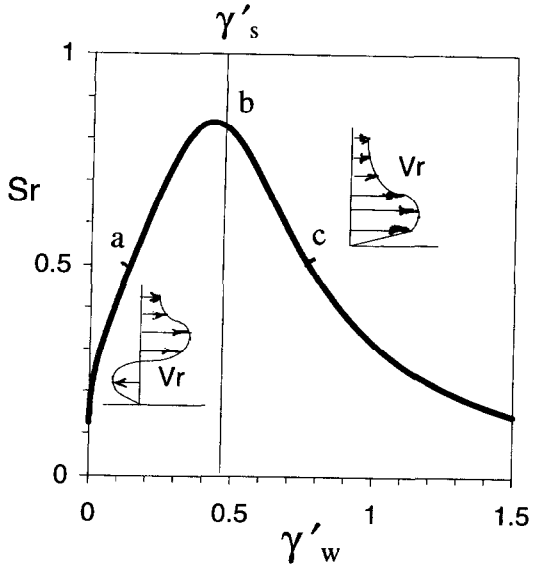

Fig. 10. Dependence of swirl ratio Sr on the swirl shear stress γ'_w. The vertical line (at b) separates the one- and two-cell flow regions. The inserts show typical profiles of the radial velocity.

interpretation of this parameter is that γ'_w is a scaled friction factor for swirl: $\gamma'_w = c_{fs} Re_s^{1/2}/2$, $c_{fs} = 2\tau_{\phi 0}/\rho v_{\phi\infty}^2$, where $\tau_{\phi 0}$ is the shear stress on the wall and $v_{\phi\infty}$ is swirl velocity far from the wall.

While the boundary layer problem has only one control parameter, γ'_w, the entire flow depends also on Re_s. Parameter A is not independent now: as follows from the solution matching, $A = -Re_s^{3/2}\Phi'(\infty)/2$, where $\Phi'(\infty)$ is known from the boundary layer problem. Since $\Phi'(\infty)$ has no evident physical meaning, we present the results using another parameter—the swirl ratio $Sr = v_{\phi\infty}/v_{rm}$, where $v_{\phi\infty}$ and v_{rm} are the maximum swirl and radial velocities as at fixed distance, $r\sin\theta$, from the axis.

Figure 10 shows the dependence of Sr on γ'_w. There is the maximum of $Sr = Sr_m = 0.839$ at $\gamma'(0) = 0.417$ and two boundary layer solutions for $Sr < Sr_m$. The radial flow is unidirectional for $\gamma'(0) > \gamma'_s = 0.467$ and there is the radial counter-flow for $\gamma'(0) < \gamma'_s$ (see the sketches in the corresponding regions separated by the vertical line, $\gamma'(0) = \gamma'_s$, in Fig 10). Figure 11 shows the velocity profiles for (a) two-cell, (b) separation and (c) unidirectional flow patterns (see the corresponding points a–c in Fig. 10).

Heat problem for the near-wall jet

Consider the case when the wall and fluid far from the wall have uniform but different temperatures, T_w and T_∞. For this problem, a temperature solution needs only one normal mode with $\alpha = m = 0$ in (5), and (6) reduces to

$$[(1-x^2)\vartheta']' = Pr\,\psi\vartheta'. \tag{28}$$

Interpreting ϑ as $(T_w - T)/(T_w - T_\infty)$ leads to the boundary conditions,

$$\vartheta = 0 \quad \text{at } x = 0 \quad \text{and} \quad \vartheta = 1 \quad \text{at } x = 1 \tag{29}$$

which are the same as those for $\gamma = \Gamma/Re_s$.

Near-wall boundary layer. For a strong jet and $Pr \geqslant O(1)$, temperature is uniform in the inviscid flow (25) and $\vartheta \equiv 1$. Inside the boundary layer (26) and (27), (28) reduces to

$$\vartheta'' = -Pr\,W\vartheta' \tag{30}$$

where the prime denotes differentiation with respect to η. Note that at $Pr = 1$, (30) coincides with equation (27) for γ. Since the boundary conditions for ϑ and γ are also the same, one does not need to solve the heat problem (28) and (29) at $Pr = 1$ because distributions of temperature and circulation coincide. In particular, the γ profiles in Fig. 11 shows also distribution of ϑ at $Pr = 1$.

Thus, the Reynolds analogy for distribution of the streamwise velocity and temperature is valid in this boundary layer. We reiterate that here v_ϕ plays the role of the streamwise velocity. To calculate heat transfer, the relation, $St = c_{fs}/2$, can be used, where the Stanton number St is a ratio of heat flux to the dynamic head [17]. Since the heat flux from the wall is proportional to the swirl shear stress, heat transfer increases with swirl.

Large Prandtl number. Now consider the case, $Pr \gg 1$, when temperature differs from its ambient value only in a thin near-wall layer even for small Reynolds numbers when there is no boundary layer for velocity. Since the thickness of this thermal layer is small compared with flow scales, we can use the first nonzero term of the Taylor expansion for ψ in the vicinity of $x = 0$, $\psi = \psi''(0)x^2/2$. Note that ψ is negative for the flow considered, e.g., see (25), and, therefore, $\psi''(0)$ is also negative. Introducing $\eta = (-\psi''(0)\,Pr/6)^{1/3}x$ and allowing $Pr \to \infty$ reduce (28) to

$$\vartheta'' = -3\eta^2\vartheta' \tag{31}$$

where the prime denotes differentiation with respect to η. The first integration yields, $\vartheta' = \exp(-\eta^3)/C_3$, and the second integration gives

$$\vartheta = \int_0^\eta \exp(-\eta^3)\,d\eta/C_3,$$

$$C_3 = \int_0^\infty \exp(-\eta^3)\,d\eta = 0.5117. \tag{32}$$

The obtained distribution of ϑ is similar to the γ distribution in Fig. 11(c). In particular, (32) results in the relation

$$Nu = C_3^{-1}(r^2\tau_{r_\theta}\rho^{-1}\nu^{-2}\,Pr/6)^{1/3}$$

$$= C_3^{-1}(c_{fr}\,Pr\,Re_s^2/12)^{1/3} \tag{33}$$

where $Nu = St\,Pr\,Re_s$ is the Nusselt number and

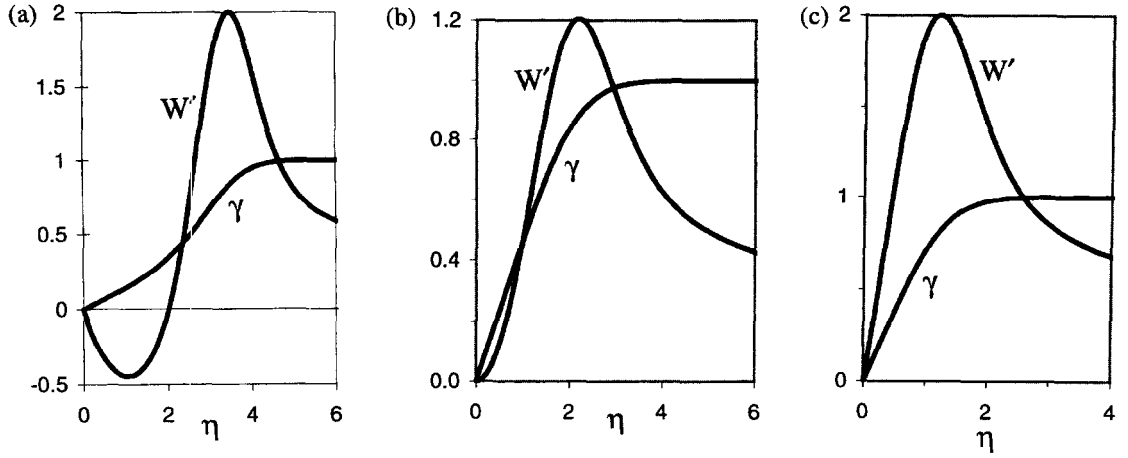

Fig. 11(a)–(c). The profiles of the radial W' and swirl γ velocities at points a, b and c in Fig. 10, respectively.

$c_{fr} = 2\tau_{r_\theta}/\rho v_{\phi\infty}^2$ is the friction factor for the radial velocity.

Since Nu is proportional to the positive power of the radial shear stress τ_{r_θ}, (33) predicts $Nu = 0$ for the separation case where $\tau_{r_\theta} = \psi''(0) = 0$ (Fig. 11(b)). For this specific flow, however, the representation for the stream function must be modified to $\psi = \psi'''(0)x^3/6$. Introducing $\eta = (-\psi'''(0)Pr/24)^{1/4}x$ and allowing $Pr \to \infty$ reduce (28) to $\vartheta'' = -4\eta^3\vartheta'$ which on integration gives

$$\vartheta = \int_0^\eta \exp(-\eta^4)\,d\eta/C_4,$$

$$C_4 = \int_0^\infty \exp(-\eta^4)\,d\eta = 0.5625,$$

$$Nu = C_4^{-1}(-\psi'''(0)\,Pr/24)^{1/4}. \qquad (34)$$

Thus, flow separation just leads to the smaller exponent in the power-law dependence of Nu on Pr—1/4 in (34) compared with 1/3 in (33). Swirl affects heat transfer for $Pr \gg 1$ by modifying the meridional flow only. However, the meridional flow becomes independent of swirl for the case considered below.

Weak swirl. Figure 10 shows that Sr decreases as γ'_w increases in the one-cell flow. This means that the swirl velocity becomes small compared with the radial velocity within the boundary layer (e.g. see Fig. 11(c)). As $Sr \to 0$, the meridional flow equation becomes uncoupled from that for swirl, and the boundary layer problem modifies. The new inner variables, $W(\eta) = -(-2A)^{-1/3}\psi$, $\eta = (-2A)^{1/3}x$, do not involve swirl, (27) transforms to

$$W' = \eta - W^2/2, \quad \gamma'' = -W\gamma' \qquad (35a, b)$$

and the energy equation retains the form of (30) but with the new η. One can see that (35a) is decoupled from (35b). Although (30) and (35b) again coincide at $Pr = 1$, temperature does not depend on swirl now.

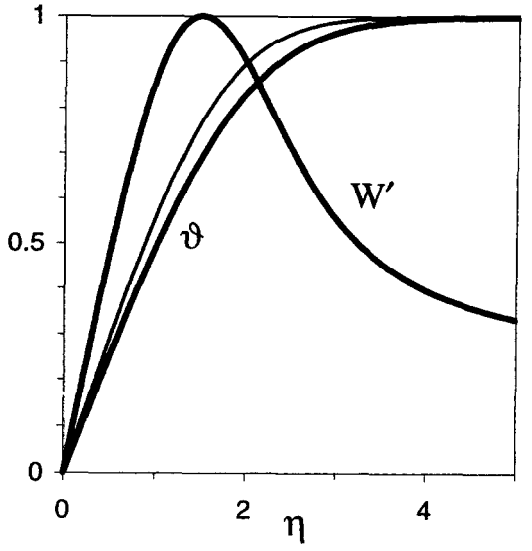

Fig. 12. The profiles of the radial W' and swirl (thin curve) velocities in the swirling near-wall jet with weak swirl. Curve ϑ shows the temperature distribution at $Pr = 0.7$.

Figure 12 shows the velocity W' and temperature ϑ profiles resulting from integration of (35). The velocity is scaled to its maximum value, $W'_m = 1.0313$, for a compact presentation. The bold curve ϑ corresponds to $Pr = 0.7$ (air) and the thin curve shows ϑ at $Pr = 1$ (and swirl velocity γ as well).

Introduce Reynolds number $Re = rv_{rm}/\nu$, where v_{rm} is the maximal radial velocity at fixed r, and friction factor $c_f = 2\tau_{r_\theta}/\rho v_{rm}^2$. The solution yields that $c_f = 2W'^{-3/2}_m Re^{-1/2}$ and $Nu = \vartheta'(0)(Re/W'_m)^{1/2}$, where $\vartheta'(0) = 0.5014$ at $Pr = 0.7$, $\vartheta'(0) = 0.579$ at $Pr = 1$ and $\vartheta'(0) \sim Pr^{1/3}$ as $Pr \to \infty$. In the latter case, ϑ is described by (31) and (32) but with $\eta = (-Pr\,A/3)^{1/3}x$, and heat transfer is governed by the relation $Nu = C_3^{-1}(Pr/6)^{1/3}(Re/W'_m)^{1/2}$.

Conical annular jet

As $\gamma'_w \to 0$, Sr also decreases (Fig. 10). The near-wall inflow (see the left insert in Fig. 10) becomes wide and, for this reason, the boundary layer approach must be modified. Consider the case where the flow cells are separated by conical surface, $x = x_s$, with $x_s \sim O(1)$. As $Re_s \to \infty$, a strong jet develops near $x = x_s = \cos\theta_s$ and the flow outside the jet is inviscid. The corresponding solutions of the Euler and boundary layer equations are:

$$\gamma \equiv 0, \quad \psi = x\,Re_s\,[(1-x_s)/(1+x_s)]^{1/2},$$

$$0 < x < x_s \quad \text{(irrotational flow region)},$$

$$\gamma = 1,$$

$$\psi = -Re_s\,\{x_s(1-x)(1-x_s^2)^{-1}[(2-x_s)x-x_s]\}^{1/2},$$

$$x_s < x \leqslant 1 \quad \text{(vortical flow region)},$$

$$\gamma = \tfrac{1}{2}(1+\tanh\xi), \tag{36a}$$

$$\psi = -x_s\,Re_s\,[(1-x_s)/(1+x_s)]^{1/2}\tanh\xi, \tag{36b}$$

(annular jet),

where

$$\xi = \tfrac{1}{2}(x-x_s)Re_s\,x_s(1-x_s^2)^{-1/2}(1+x_s)^{-1}.$$

Solution (36a) is also a uniform approximation for swirl in the entire region, $0 < x < 1$. The radial velocity, $u = Re_m\cosh^{-2}\xi$, $Re_m = \frac{1}{2}Re_s^2(1+1/x_s)^{-2}$, dominates swirl in the annular jet and $Sr = 2(1+1/x_s)^2\ Re_s^{-1}$ tends to zero as $Re_s \to \infty$. Here, x_s is a relevant control parameter while $A = -\frac{1}{2}Re_s^2\ (1+1/x_s)^{-1}$.

The boundary-layer reduction of (28) for the annular jet is

$$\vartheta'' = -2\,Pr\,\vartheta'\tanh\xi \tag{37}$$

where the prime denotes differentiation with respect to ξ. The first integration of (37) yields $\vartheta' = C(\cosh\xi)^{-2Pr}$ and the second integration gives

$$\vartheta = -\int_{-\infty}^{\xi}(\cosh\xi)^{-2Pr}\,d\xi \Big/ \int_{-\infty}^{\infty}(\cosh\xi)^{-2Pr}\,d\xi. \tag{38}$$

The inviscid solutions for ϑ are the same as those for γ, i.e. $\vartheta \equiv 0$ for $0 < x < x_s$ and $\vartheta \equiv 1$ for $x_s < x \leqslant 1$. So that (38) is a uniform approximation for temperature in the entire region, $0 < x < 1$.

At $Pr = 1$, (38) reduces to $\vartheta = \frac{1}{2}(1+\tanh\xi)$, and the profiles of ϑ and γ (36a) coincide. For $Pr \gg 1$, (38) reduces to $\vartheta = \frac{1}{2}[1+\mathrm{erf}(Pr^{1/2}\xi)]$. Thus, temperature is uniform (but different) in both the inviscid regions and there is a temperature front (region of a high temperature gradient) near the separating surface, $x = x_s$.

Consider a cylindrical surface, $r\sin\theta = \text{const}$. On this surface, the swirl velocity v_ϕ and ϑ are zero below the jet and are constant and equal to their ambient values above the jet. Since the profiles, v_ϕ and ϑ coincide across the jet as well, the distributions of the swirl velocity and temperature are the same on the entire cylindrical surface. Both swirl and ambient temperature are 'locked' in the upper flow cell while near the wall, the flow is swirl-free and the fluid has the wall temperature. Therefore, increasing swirl suppresses wall heat transfer in the two-cellular regime, i.e. provides the opposite effect compared with the near-wall swirling jet.

DISCUSSION

The role of swirl in heat processes

We have obtained a few exact solutions of the energy equation for (i) a point heat source and (ii) wall–fluid heat exchange which explain some of the important effects of swirl on convective heat transfer. These effects are:

(a) *Significant increase in heat (and mass) transfer.* For heat diffusion from a hot submerged jet to a cold ambient fluid considered in problem (i), the maximal temperature decays (as the distance from the source increases) significantly faster in a swirling jet than in a swirl-free jet. As analytical solutions (15)–(16) show, the maximal temperature is inversely proportional to the swirl Reynolds number Re_s. The enhanced heat exchange occurs due to the development of the swirl-induced recirculatory cell that drastically increases the area of a contact surface between the jet and ambient fluid.

Swirl also increases heat transfer from a wall as shown in problem (ii). At $Pr = 1$ and fixed swirl ratio Sr, heat flux is proportional to the swirl friction. For $Pr \gg 1$, heat flux is proportional to $Pr^{1/3}$ or $Pr^{1/4}$ depending on the flow pattern as solutions (32)–(34) show.

(b) *Heat isolation of a wall.* On the other hand, swirl can cause flow separation from a wall that leads to the opposite effect—significant decrease in heat transfer. The flow is composed of a near-wall cell, where temperature is nearly equal to that of the wall, and an outer cell, where temperature is close to its value at infinity. For such flow patterns, heat transfer exponentially decays as $Re_s \to \infty$ and, therefore, swirl can be used for heat isolation of wall.

(c) *Development of a temperature front.* Between the flow cells considered in the problem (ii), there is a thin layer ('front') where temperature varies from the ambient to the wall values. Such a temperature front is observed in natural (tornadoes, firestorms and other meterological streams) and technological (vortex burners and chemical reactors) flows. The physical mechanism of the front development is heat convection by the flow converging toward the front from both sides (cells). The analytical solution (38) describes the temperature distributions in the conical front, $\theta = \theta_s$, depending on Re_s, Pr and θ_s.

(d) *Stabilization of heat and mass transfer.* Effects (a) and (c) are useful for stabilization of heat and mass transfer, e.g. in vortex burners, where fuel is supplied by a swirling jet issuing from a nozzle into a combustion chamber [18]. In the jet vicinity, the flow is similar to that shown in Fig. 3, and isolines of fuel concentration is similar to isotherms shown in Fig. 5(d) (note that solutions (15) and (16) can be applied to the diffusion equation as well). The reversed flow in the near-axis cell transports heat upstream of combustion region, forming the temperature front. This enhances fuel pre-heating and thus stabilizes combustion. The solutions obtained can be used for prediction and optimization of these processes (using a uniform eddy viscosity to model turbulence). The approach can be developed further to incorporate combustion prediction inside the temperature front.

Thus, our solutions explain the mechanism and the influence of control parameters on effects (a)–(d). Another interesting result relates to the validity of the Reynolds analogy in swirling flows, discussed below.

Reynolds analogy

The analogy between velocity and temperature distributions is an important feature of boundary layers allowing evaluation of heat transfer based only on the flow characteristics. The analogy holds at $Pr = 1$ (which is a typical value for turbulent flows) due to the similarity of equations and boundary conditions for both. Usually, there is similarity for temperature and longitudinal velocity in near-wall boundary layers.

The Reynolds analogy is valid here for the annular conical jet in problem (i) where the profiles of the radial velocity and temperature coincide. The centrifugal force is exactly balanced by the pressure gradient in the annular jet. This makes the boundary layer equations for the radial velocity and temperature identical. The analogy disappears when the annular jet transforms into the Long (near-axis) jet. In this boundary layer problem, the centrifugal force is not balanced by the pressure gradient only, the momentum equations are coupled, and the velocity and temperature profiles are qualitatively different (see Fig. 7(b)–(d)). The analogy is restored as the flow transforms from the Long to the Schlichting swirl-free jet (Fig. 7(a)).

It is interesting that in the problem (ii), there is the analogy between temperature and the swirl (but not radial!) velocity distributions. This analogy occurs for both the annular jet and near-wall boundary layer. Swirl and temperature profiles coincide even for the cases where the radial velocity dominates swirl (in the annular jet and in the near-wall layer for weak swirl). Moreover, the analogy is valid not only inside the jet but also in the entire region for the two-cell flow as $Re_s \to \infty$.

CONCLUSION

Two heat problems for conical swirling jets are solved describing heat diffusion from the point source and heat transfer between a wall and ambient fluid. The analytical solutions obtained explicitly show the important effects of swirl which either enhances or suppresses heat exchange depending on the control parameters. These results are not only of scientific interest (being unique analytical solutions for heat transfer in swirling flows) but can also be utilized for technological applications (e.g. in vortex burners and chemical reactors).

Acknowledgements—This research was founded by the Air Force Office of Scientific Research Grant F49620-95-1-0302. The authors are grateful to Professor A. I. Leontiev and Prashant Haldipur for valuable discussions.

REFERENCES

1. Gupta, A. K., Lilley, D. G. and Syred, N., *Swirl Flows*, Chap. 1. Abacus Press, New York, 1984.
2. Hussain, F., Goldshtik, M. and Yao, R. J., The vortex liquid piston engine and some other vortex technologies. *Proceedings of Seminar on Fluid Mechanics Research*. Dhaka, Bangladesh, 1995, pp. K75–K108.
3. Cheng, R. K., Velocity and scalar characteristics of premixed turbulent flames. *Combustion and Flame*, 1995, **101,** 1–14.
4. Cutler, A. D, Levey, B. S. and Kraus, D. K., Near-field flow of supersonic swirling jets. *AIAA Journal*, 1995, **33,** 876–881.
5. Fulton, C. D., Ranque's tube. *Refr. Eng.*, 1950, **58,** 473–479.
6. Borissov, A. A., Kuibin, P. A. and Okulov, V. L., Calculation of the Ranque effect in the vortex tube. *Acta Mechanica, Suppl.*, 1994, **4,** 289–295.
7. Rumer, Yu. B., Convective diffusion in a submerged jet. *J. Appl. Math. and Mech.*, 1953, **17,** 743–744.
8. Shtern, V. and Hussain, F., Hysteresis in swirling jets. *Journal of Fluid Mechanics*, 1996, **309,** 1–44.
9. Schlichting, H., *Boundary-Layer Theory*, 6th edn. McGraw-Hill, New York, 1968, p. 218.
10. Squire, H. B., The growth of vortex in turbulent flow. *Aero. Quart.*, 1965, **16,** 302–306.
11. Govindaraju, S. P. and Saffman, P. G., Flow in a turbulent trailing vortex. *Physics of Fluids*, 1971, **14,** 2074–2080.
12. Burrgraf, O. R. and Foster, M. R., Continuation of breakdown in tornado-like vortices. *Journal of Fluid Mechanics*, 1977, **80,** 685–704.
13. Serrin, J., The swirling vortex. *Phil. Trans. R. Soc. Lond. A*, 1972, **271,** 325–360.
14. Rohsenow, W. N. and Hartnett, J. P., *Handbook of Heat Transfer*. McGraw-Hill, New York, 1973.
15. Long, R. R., A vortex in a infinite viscous fluid. *Journal of Fluid Mechanics*, 1961, **11,** 611–623.
16. Gregory, N., Stuart, J. T. and Walker, W. C., On the stability of three dimensional boundary layers with application to the flow due to a rotating disk. *Phil. Trans. R. Soc. Lond. A.*, 1995, **248,** 155–199.
17. Eckert, E. R. G. and Drake, Jr, R. M., *Analysis of Heat and Mass Transfer*. McGraw-Hill, New York, 1972.
18. Keller, J. J., Sattelmayer Th. and Thüringer, F., Double-cone burner for gas turbine type 9 retrofit application. *Proceedings of the 19th International Congress on Combustion Engines*, CIMAC 1991, Florence, Italy.